Bio-based, self-adhesive, and self-healing ionogel with excellent mechanical properties for flexible strain sensor†

Yipeng Zhang,[a] Junhuai Xu[b] and Haibo Wang (ID) *[bc]

Bio-based ionogels with versatile properties are highly desired for practical applications. Herein, we designed a novel self-healing, anti-freezing, and self-adhesive ionogel with excellent sensor capability. The ionogel was obtained by cross-linking amino groups (chitosan) and aldehyde groups (dextran oxide) to form Schiff-base bonds in the ionic liquids (EMIMOAc) with TA. Ionogels inherited the superior electrical conductivity of ionic liquids (IG$_2$, 1.1 mS cm^{-1}). Due to the dynamic reaction of Schiff-base bonds, the obtained IG$_2$ possessed self-healing properties (self-healing efficiency = 89%). The presence of TA also provided the ionogel with excellent self-adhesive properties (IG$_2$/TA, adhesive strength to hogskin = 8.05 kPa). Owing to the low freezing point and low vapor pressure of ionic liquids, ionogels were endowed with anti-freeze properties and resistance to solvent volatility. Moreover, the ionogel can act as a strain sensor, and exhibited excellent sensitivity and sensing performance. Our work provided a green and effective method in preparation of the high performance ionogel sensor, which could accommodate future practical industrial applications.

Introduction

With the development of science and technology, wearable smart devices have been widely introduced into people's vision. The demand for smart sensors has also risen dramatically, and various smart bionic devices have been developed to be widely used at the human–machine interface, in electronic skin, and personalized medicine. Among them, gel-based sensors have received wide attention due to their excellent electrical conductivity and good flexibility and tensile properties.[1–6]

Nowadays, common hydrogels are widely studied because of their simple preparation, but they all inevitably suffer from evaporation of solvent water or freezing of water at temperatures below zero, which would seriously affect the performance of the sensor. Ionogels, unlike common hydrogels, are mainly composed of ionic liquids and polymers. Due to the inherent properties of ionic liquids (high ionic conductivity, low freezing point, high boiling point, *etc.*) being retained, the resulting ionogels have excellent ionic conductivity and are resistant to both volatility and freezing. This is a great improvement over conventional hydrogels. Meanwhile, due to the shortage of

fossil resources and environmental degradation, scientists are gradually turning their interest to renewable and eco-friendly biomass materials. Natural polymers such as cellulose,[7–12] sodium alginate,[13–16] dextran[17,18] and chitosan[19,20] have been widely used in the preparation of polymer products to replace synthetic polymers. Wang *et al.*[12] fabricated an ionogel by cellulose and ionic liquid, which had obvious advantages over the existing equivalent products in terms of mechanical and electrical conductivity. And it can perform well under high and low temperature conditions.

The self-healing sensors would automatically repair mechanical and electronic damage under environmental conditions. As a result, the durability and reliability of gel-based sensors could be enhanced by introducing the self-healing property. A variety of self-healing mechanisms have been used to synthesize self-healing sensors, such as covalent bonds (borate bonds,[21–23] Schiff base bonds,[24] *etc.*) and non-covalent bond interactions (ionic bonds,[25,26] hydrogen bonds[27,28] and host–guest interaction[29,30] *etc.*). Among them, covalent bonds are widely preferred due to the superiority of the mechanical properties of the prepared materials over those of non-covalent bonds. For example, the self-healing sensors based on Schiff-bond by Peng *et al.* had excellent self-healing properties.[31]

Although promising progress has been made, current flexible sensors are usually difficult to fit well with the human body, and require tape to be fixed on human skin or clothing, leading to an unstable signal as a human motion sensor. Therefore, good adhesion performance will be one of the necessary properties of future sensors. Inspired by nature, dopamine,

[a] West China Hospital of Sichuan University, Chengdu 610041, China

[b] College of Biomass Science and Engineering, Sichuan University, Chengdu 610065, P. R. China. E-mail: whb6985@scu.edu.cn

[c] National Engineering Research Center of Clean Technology in Leather Industry, Sichuan University, Chengdu 610065, PR China

a derivative of mussel material, can be used as an adhesion agent to develop hydrogels with special tissue adhesion properties.[32] But the high cost of dopamine also makes it highly limited in practical applications. Tannic acid (TA) is an inexpensive polyphenolic substance that has a similar structure to dopamine and has significant adhesion to different surfaces, making it an ideal substitute for dopamine.[33]

Herein, based on the concept of environmental protection, we tried to develop a fully bio-based ionogel with excellent adhesion properties and self-healing properties. Dextran oxide (containing aldehyde groups) was co-dissolved with chitosan in IL, and TA was also uniformly dispersed in it. The ionogels were obtained through the reaction of aldehyde groups with amino groups (Schiff base bond structure). The uniform distribution of IL in ionogels would give them excellent conductivity, anti-volatility, and anti-freeze properties. Meanwhile, the dynamic Schiff base bonds in the cross-linked network would also confer good self-healing properties to the ionogels. The addition of TA increases the adhesion properties of the ionogel and allows for a perfect fit directly on the object. We believe that this fully bio-based ionogel sensor has potential for a wide range of applications.

Experiments

Materials

Ionic liquid of 1-ethyl-3-methylimidazolium acetate (EMIMOAc) was purchased from Sigma-Aldrich. Sodium periodate ($NaIO_4$), dextran (M_w = 40 kDa), chitosan (M_w = 100–300 kDa, deacetylation degree = 95%) and tannic acid (TA) were purchased from Admas-beta. Other reagents were obtained from Chron Chemicals Co., Ltd.

Instrumentations

The morphology of ionogels was observed by a scanning electron microscope (SEM). The sample was soaked in water for five days to completely replace the IL in the gel, and then freeze-dried for SEM. A TA-AR2000EX stress-controlled rheometer (TA Instruments) was used to conduct the rheological measurements. The dynamic temperature sweep measurements at a fixed angular frequency were conducted from 25 to 160 °C with a heating rate of 2 °C min^{-1}. All measurements were conducted under a nitrogen atmosphere. The ionic conductivities (σ_i) of the ionogels were determined by the AC impedance spectroscopy (Zahner Zennium pro) with an the two-point probe. 10 mV of the voltage amplitude was applied in the frequency range from 100 kHz to 0.1 Hz. Fourier transform infrared (FTIR) spectra were acquired with a PerkinElmer FTIR spectrometer (the scan wavelength ranges from 400 to 4000 cm^{-1}, scanning number of 32 times, resolution of 4 cm^{-1}). The mechanical properties were performed by a tensile test machine (Instron 4465) at the stretching rate of 20 mm min^{-1}. The digital images were captured using a Nikon D7100 camera.

Preparation of dextran oxide

5 g of dextran was dissolved in phosphate buffer solution at pH = 5.6, and equimolar amounts of sodium periodate (relative to glucose units on dextran) were then added to the solution, stirred at 1500 rpm for 2 h at room temperature, and appropriate amounts of propanetriol were added. Subsequently, after continuing stirring for 15 min, it was introduced into a dialysis bag, dialyzed with water as the medium for two days, and freeze-dried to obtain oxidized dextran.

Synthesize of ionogels

A certain quantity of chitosan was dissolved in EMIMOAc to obtain a homogeneous and transparent solution. Then, the chitosan solution and the dextran oxide solution were mixed in a certain proportion. Finally, TA was dissolved in the solution to obtain a homogeneous mixture. The final mixture was transferred to a PTFE mold, and then placed in an oven at 80 °C to form gelation *via* Schiff-base reaction. The preparation procedure is shown in Fig. 1. The Table 1 was exhibited the content of each part in the ionogels (5 wt%, 10 wt%, 15 wt%, named as IG_1, IG_2, IG_3).

Results and discussion

Synthesis of chitosan/dextran–TA ionogels

Dextran oxide was chemical crosslinked with chitosan *via* Schiff base reaction in homogeneous ionic liquid solution to obtain chitosan/dextran–TA ionogels. First, partial hydroxyl groups of dextran were oxidized to aldehyde groups. Subsequently, self-healable and self-adhesive ionogel was prepared by chemically cross-linked between chitosan and dextran. The FTIR spectra of the chitosan, original dextran, dextran oxide, EMIMOAc, and chitosan/dextran–TA ionogel were clearly exhibited in Fig. 2a.

The strong band at 3350 cm^{-1} was assigned to the –OH of these bio-based polymer (chitosan, dextran, and dextran oxide). The characteristic peaks at 1664 cm^{-1} and 1593 cm^{-1} can be attributed to the twisting and wagging vibration of the –NH$_2$
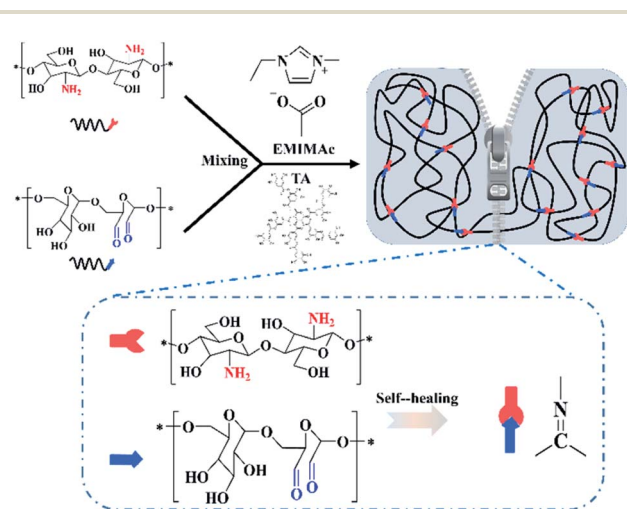

Fig. 1 Illustration of ionogel preparation routine.

Table 1 Ratio of each part of different ionogels

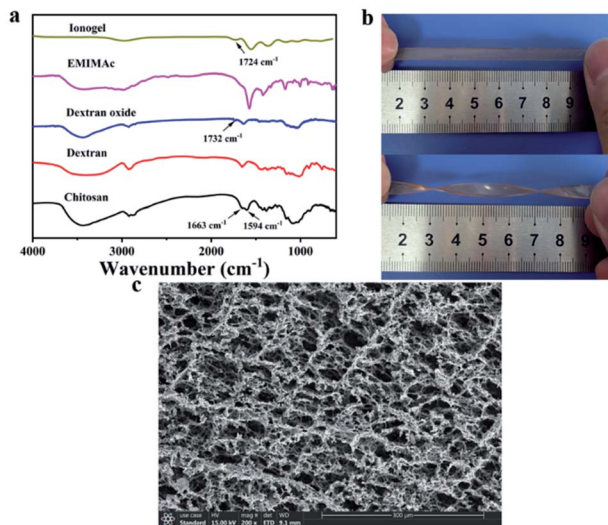| Samples	Amount of dextran/wt%	Amount of chitosan/wt%	Amount of TA/wt%	Amount of IL/wt%
IG_1	2.5	2.5	0	95
IG_2	5	5	0	90
IG_3	7.5	7.5	0	85
IG_2/TA	5	5	1	90

Fig. 2 The characterizations of ionogel: (a) FT-IR spectrum; (b) photos of the ionogel (IG_2) with different shape (twisted and stretched); (c) SEM photos of IG_2.

(chitosan). For dextran oxide, a band compared to dextran at 1732 cm^{-1} was assigned to the C=O group. As for the cross-linked ionogel, the characterization peaks of chitosan (–NH$_2$) and dextran oxide (C=O) was decreased or disappeared. Meanwhile, the characteristic peak of C=N groups can be observed at 1724 cm^{-1}. Due to the small amount of TA, its characteristic peak cannot be observed in this spectrum.

Morphology of ionogels

Since the prepared ionogels are flexible, the ionogel can be stretched and twisted into different shape. Fig. 2b showed the photos of the ionogels with different states of ionogels. To image the morphology of the ionogel, the samples were first subjected to a series of pre-treatments and freeze-dried for the observation of SEM. As shown in Fig. 2c, the inner of the samples was extremely coarse and contains a large number of micron-sized pores. This special porous structure provided a good ion channel for ion transport, allowing the ionogel to possess excellent ionic conductivity.

Rheological and mechanical properties of ionogels

The changes of storage modulus (G') and loss modulus (G'') as a function of angular frequency for different ionogels was shown in Fig. 3a. The values of G' were always higher than that of G'', and both the G' and G'' were almost independent with the

frequency. These results indicated a typical gel behavior of the ionogels. Low thermo-mechanical stability is a common problem for gels in general, but this problem can be better solved by chemically cross-linked gels. As with the obtained IG_2, they were quite stable and the value of G' could be maintain over a wide range of temperature (25 to 120 °C, Fig. 3b). Importantly, the gel state structure would not be destroyed at temperature up to 150 °C, which can be demonstrated by dynamic temperature sweep measurements. The typical stress–strain curves of the tensile tests for the obtained ionogels.

As shown in Fig. 4a, the strain strength increased from 120 kPa to 435 kPa, which was corresponding with the polymer contents. The above results were mainly attributed to the cross-linking densities. While the strain strength and elongation at break decreased with the polymer contents. The strain strength and elongation at break of IG_2 were 332 kPa and 443%, respectively. As for IG_3, the strain strength increased to 435 kPa and the elongation at break decreased to 334%. The outcomes can be explained by the cross-linking density increased with increasing polymer contents. The information of the storage modulus and tan delta for IG_2 was provided by dynamic mechanical analysis. The change of storage modulus and tan delta of IG_2 was shown in Fig. 4b. Besides, the mechanical properties of IG_2 with and without TA were conducted, and the results revealed that the tensile strength of the ionogel became slightly stronger after the addition of TA, but the elongation at break decreased slightly (Fig. S1†). This may be due to the increased hydrogen bonding within the ionogel due to the addition of TA, resulting in an increase in tensile strength and a decrease in elongation at break. In the temperature range between −90 °C and 100 °C, the storage moduli of IG_2 first sharply decreased, and then almost kept the same. Furthermore, the T_g of IG_2 was around −60 °C, indicating that the
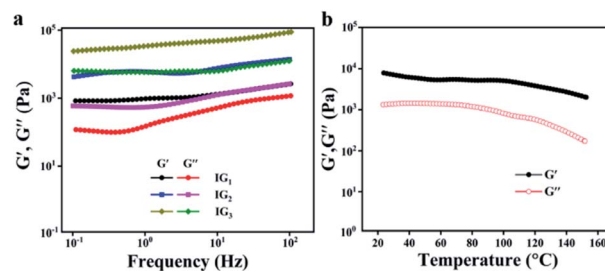

Fig. 3 Rheological properties of ionogels: (a) the relationship between storage modulus (G'), loss modulus (G'') and angular frequency for different ionogels; (b) the relationship between storage modulus (G'), loss modulus (G'') and temperature for IG_2.
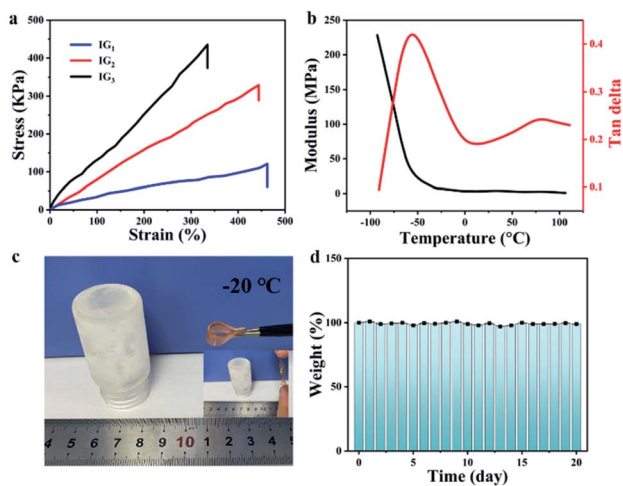
Fig. 4 The mechanical properties and thermal stability: (a) the mechanical properties of different ionogels; (b) dynamic mechanical properties of ionogel from −90 to 110 °C; (c) photo of the ionogel at −20 °C; (d) the weight of ionogel in air varies with the days.

obtained ionogels can work at extremely conditions (temperature at sub-zero). The ionogel at −20 °C also can keep flexible (Fig. 4c and d), which was further proved the anti-freezing ability of ionogels. Therefore, ionogel with such excellent properties (good mechanical strength, outstanding thermal stability) over a wide temperature range demonstrated that it can work as a superior sensing material in extreme environments.

Self-healing properties of ionogels

To maximize the service life of materials and reduce maintenance costs, the self-healing feature of materials is highly desirable in practical applications. The dynamically reversible C=N double bonds endow the chemically cross-linked ionogels with excellent self-healing properties as illustrated in Fig. 5. A rectangular ionogel sample strip was cut and then tightly contacted together. After one day at room temperature, or 5 hours at 50 °C, the fracture disappeared and the healed strip can be stretched again to several times its original length (Fig. 5a). POM was further used to demonstrate the self-heal process of the ionogel, as shown in the Fig. 5b, where the cracks were gradually healed with time. It was attributed to the re-bonding
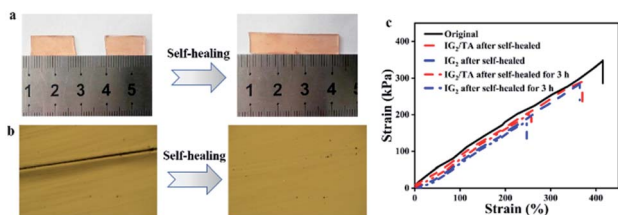
of the broken C=N double bonds, resulting the repair of the ionogel. The infrared spectroscopy characterization of the ionogels before and after self-healing demonstrated that the intensity of the C=N peak at 1724 cm^{-1} gradually increased with increasing healing time, indicating that the bond was being re-generated (Fig. S2†). The self-healability of these ionogels was also investigated by comparing their mechanical properties original and healed, and the results were illustrated in Fig. 5c. The repair efficiency of the ionogel containing TA was initially significantly higher than that of the ionogel without TA, due to the strong adhesive properties of TA in the ionogel, which caused a certain force between the fractured ionogels. When the repair procedure was completed, the repair efficiency of the two ionogels was almost identical, as the effect of TA on the adhesion between the two broken ionogels was negligible once the C=N was re-bonded together. The self-healing efficiency (η) of ionogels grows with increasing healing time, and can exceed 89% when the self-healing time is over 1 day at room temperature, or over 5 hours at 50 °C. The variation of the time of self-healed *versus* mechanical properties in the Fig. S3† exhibited that the mechanical properties of the healed ionogel gradually decrease as the time of self-healed increases. And after 5 times, the efficiency was already below 60%. (Self-healing efficiency is defined as η = healed strength/original strength.)

Self-adhesive ability of ionogels

To ensure accurate sensor monitoring, it is essential to improve the adhesion between human skin and wearable devices adhesion between electronic devices. A good adhesion between the skin and the sensor can avoid interface delamination of the sensor during repeated dynamic deformations, which can lead to inaccurate detection. To this end, TA was introduced to endow the ionogel with the unique self-adhesive ability. The TA was added into IG$_2$ as the example (IG$_2$/TA).

As displayed in Fig. 6, the IG$_2$/TA exhibited strong adhesion to diverse objects, including inorganic materials and organic materials (Fig. 6a). More interestingly, the ionogel can be completely and easily peeled off from the attached objects without any residues (Fig. 6b). The adhesive strength of the ionogel to plastic, glass, PTFE and hogskin was up to 22.63, 19.72, 10.41 and 8.05 kPa, respectively (Fig. 6c). These exciting results demonstrated its great potential for wearable applications.
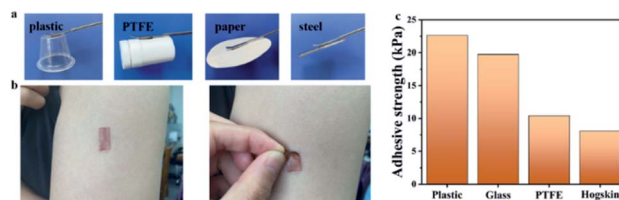

Fig. 5 The self-healing ability of ionogels: (a) the photos of self-healed ionogel; (b) the POM photos of self-healing process; (c) the mechanical properties of ionogel before and after self-healed.

Fig. 6 Adhesive ability of ionogels: (a) ionogel adhered to different materials (inorganic materials and organic materials); (b) the ionogel could easily peel off from the attached objects without any residues; (c) the adhesive strength of the ionogel to plastic, glass, PTFE and hogskin.

Sensor capability of ionogels

Since the vast majority of the components of ionogels are composed of ionic liquids, ionogels should have the excellent electrical conductivity that ionic liquids possess. Numerous literature reports on ionogels prepared based on ionic liquids also support this view. The EMIMOAc was closed to use as the matrix owing to its excellent solubility for chitosan and dextran, and non-toxic to humans.[34,35] Hence, a strain sensor with a size of $2 \times 1 \times 0.3$ cm^3 was fabricated. The correlation between the strain length and the resistance variations was measured. As exhibited in Fig. 7a, the resistance of the sensor increased as it gradually stretched. The gauge factor (GF) was then calculated by the ratio of relative change in electrical resistance R to the mechanical strain $\varepsilon \left(\mathrm{GF} = \dfrac{(R - R_0)/R_0}{\varepsilon} \right)$. The GF for the IG$_2$/TA sensor was increased from 0.19 to 0.44, as the strain was varied from 0% to 290% (Fig. 7b). These values were much better than many previously reported sensors. Since the ionogel had a T_g of $-60\,^\circ$C and remained flexible at $-20\,^\circ$C, the ionogel as a sensor with excellent freeze resistance should exhibit stable sensing performance at low temperatures. Therefore, the sensing performance of ionogel at different temperatures was compared. As shown in Fig. 7c, the ionogel presented almost the same resistance change at $-20\,^\circ$C, $0\,^\circ$C, $20\,^\circ$C. All the results discussed above indicated that the obtained ionogel sensor can provide reliable sensing performance under different conditions. Due to the wide working range, excellent mechanical, and adhesion properties of ionogel sensor, the feasibility of the ionogel sensor as wearable sensor was discussed for diverse human motions. Fig. 7d showed the ionogel sensor was used to monitor the wrist bending state. The relative resistance change of the sensor was clear and stable under different states (bending up, original state, bending down). Moreover, the different states of the elbow (Fig. 7e) could also be detected by the relative variations of the resistance of the ionogel sensor. Similarly, the ionogel sensor also be attached to the knee to monitor the movement of the joint (Fig. 7f). To demonstrate the sensing stability of ionogel after storage for a period of time, the strain sensing performances were conducted (Fig. S4†). Obviously, the results exhibited that the sensing performance of the ionogel remained unchanged with time.

Conclusion

In this paper, we synthetized a new type of dynamic chemical cross-linked ionogels based on bio-macromolecular polymers (chitosan and dextran) in ionic liquid. The ionogel obtained by Schiff base reaction had good mechanical properties (strain strength and elongation at break of IG$_2$ were 342 kPa and 414%), and was endowed with a better self-healability. TA enabled the ionogel to have excellent adhesion to different surfaces. The DMA tests indicated that the ionogels could maintain outstanding flexibility when the temperature was below zero. What's more, owing to the good conductivity of ionogel at different temperature, it was used as a flexible ionogel strain sensor. The ionogel showed good sensing performance under different conditions and environment (GF = 0.19 to 0.44). Therefore, the prepared self-healable, self-adhesion and anti-freezing ionogels are promising as an ideal flexible strain sensor under different conditions.

Conflicts of interest

There are no conflicts to declare.

Acknowledgements

Notes and references

1 H. C. Jing, L. Xu, X. Q. Wang, Y. Q. Liu and J. C. Hao, *J. Mater. Chem. A*, 2021, **9**, 19914–19921.
2 S. Hong, Y. Yuan, C. Z. Liu, W. M. Chen, L. Chen, H. L. Lian and H. Liimatainen, *J. Mater. Chem. C*, 2020, **8**, 550–560.
3 S. Xia, S. X. Song, Y. Li and G. H. Gao, *J. Mater. Chem. C*, 2019, **7**, 11303–11314.
4 P. Nedeljko, M. Turel and A. Lobnik, *Sens. Actuators, B*, 2017, **246**, 1066–1073.
5 S. Kumar, K. Namura and M. Suzuki, *Proc. SPIE*, 2019, **10894**, 1089414.
6 Y. Hu, M. Zhang, C. R. Qin, X. Y. Qian, L. N. Zhang, J. P. Zhou and A. Lu, *Carbohydr. Polym.*, 2021, **265**, 118078.
7 S. D. Yang, L. Chen, S. Liu, W. J. Hou, J. Zhu, P. Zhao and Q. Zhang, *J. Hazard. Mater.*, 2021, **408**, 124408.
8 X. Guan, Z. N. Hou, K. Wu, H. R. Zhao, S. Liu, T. Fei and T. Zhang, *Sens. Actuators, B*, 2021, **339**, 129879.
9 Y. Jiao, K. Y. Lu, Y. Lu, Y. Y. Yue, X. W. Xu, H. N. Xiao, J. Li and J. Q. Han, *Cellulose*, 2021, **28**, 4295–4311.
10 Z. X. Pei, Z. W. Yu, M. N. Li, L. J. Bai, W. X. Wang, H. Chen, H. W. Yang, D. L. Wei and L. X. Yang, *Int. J. Biol. Macromol.*, 2021, **179**, 324–332.
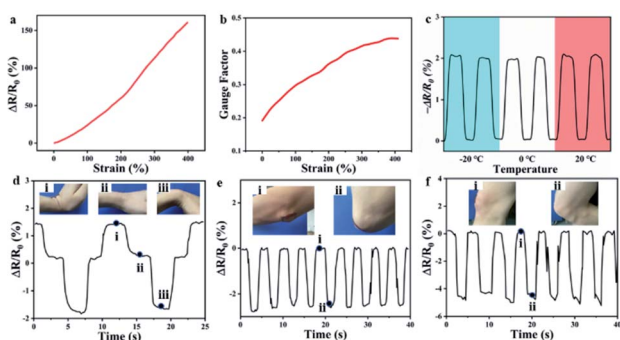

Fig. 7 The sensor capability of ionogel: (a) the relationship between $\Delta R/R_0$ and strains; (b) the value of GFs from 0 to 400% strains; (c) the sensor capability of the ionogel at different temperature; (d) the changes of resistance for bending wrist; (e) the changes of resistance for bending arm; (f) the changes of resistance for bending leg.

11 S. Wang, J. Xiang, Y. G. Sun, H. L. Wang, X. S. Du, X. Cheng, Z. L. Du and H. B. Wang, *Carbohydr. Polym.*, 2021, **261**, 129879.

12 Z. Wang, J. Liu, J. Zhang, S. Hao, X. Duan, H. Song and J. Zhang, *Cellulose*, 2020, **27**, 5121–5133.

13 Y. L. Feng, H. Wang, J. H. Xu, X. S. Du, X. Cheng, Z. L. Du and H. B. Wang, *J. Hazard. Mater.*, 2021, **416**, 125777.

14 X. J. Yun, Q. T. Zhang, B. Luo, H. R. Jiang, C. Z. Chen, S. F. Wang and D. Y. Min, *Electroanal*, 2020, **32**, 2282–2289.

15 Y. Q. Li, X. H. Liu, Q. Gong, Z. B. Xia, Y. Yang, C. Chen and C. H. Qian, *Int. J. Biol. Macromol.*, 2021, **172**, 41–54.

16 L. Zhao, Z. J. Ren, X. Liu, Q. J. Ling, Z. J. Li and H. B. Gu, *ACS Appl. Mater. Interfaces*, 2021, **13**, 11344–11355.

17 O. Tabasi, C. Falamaki and M. Mahmoudi, *Plasmonics*, 2019, **14**, 1145–1159.

18 J. Ding, Z. Qiao, Y. S. Zhang, D. R. Wei, S. P. Chen, J. J. Tang, L. Chen, D. Wei, J. Sun and H. S. Fan, *Carbohydr. Polym.*, 2020, **247**, 116686.

19 R. N. Jin, J. J. Xu, L. J. Duan and G. H. Gao, *Carbohydr. Polym.*, 2021, **268**, 118240.

20 X. Y. Hong, H. Ding, J. Li, Y. Y. Xue, L. Y. Sun and F. C. Ding, *Polym. Adv. Technol.*, 2021, **32**, 3050–3058.

21 J. H. Xu, H. Wang, X. S. Du, X. Cheng, Z. L. Du and H. B. Wang, *ACS Appl. Mater. Interfaces*, 2021, **13**, 20427–20434.

22 A. Breuillac, A. Kassalias and R. Nicolaÿ, *Macromolecules*, 2019, **52**, 7102–7113.

23 J. Xu, H. Wang, X. Du, X. Cheng, Z. Du and H. Wang, *Chem. Eng. J.*, 2021, **426**, 130724.

24 F. Parchegani, S. Amani and M. Zendehdel, *Spectrochim. Acta, Part A*, 2021, **255**, 119714.

25 G. J. Mohr, *Anal. Bioanal. Chem.*, 2006, **386**, 1201–1214.

26 H. P. Huang, J. Q. Zhang, R. C. Wang and Y. S. Qian, *Appl. Math. Inf. Sci.*, 2014, **8**, 597–605.

27 A. Wang, Y. F. Wang, B. Zhang, K. N. Wan, J. X. Zhu, J. S. Xu, C. Zhang and T. X. Liu, *Chem. Eng. J.*, 2021, **411**, 128506.

28 H. Y. Qiao, P. F. Qi, X. H. Zhang, L. A. Wang, Y. Q. Tan, Z. H. Luan, Y. Z. Xia, Y. H. Li and K. Y. Sui, *ACS Appl. Mater. Interfaces*, 2019, **11**, 7755–7763.

29 S. Tarasi, A. A. Tehrani and A. Morsali, *Sens. Actuators, B*, 2020, **305**, 127341.

30 X. Liu, Z. J. Ren, F. F. Liu, L. Zhao, Q. J. Ling and H. B. Gu, *ACS Appl. Mater. Interfaces*, 2021, **13**, 14625–14635.

31 W. Peng, L. Han, H. Huang, X. Xuan, G. Pan, L. Wan, T. Lu, M. Xu and L. Pan, *J. Mater. Chem. A*, 2020, **8**, 26109–26118.

32 C. Zhang, Y. S. Zhou, H. J. Han, H. X. Zheng, W. H. Xu and Z. K. Wang, *ACS Nano*, 2021, **15**, 1785–1794.

33 S. W. Hao, C. Y. Shao, L. Meng, C. Cui, F. Xu and J. Yang, *ACS Appl. Mater. Interfaces*, 2020, **12**, 56509–56521.

34 A. Hijo, H. Barros, G. Maximo, C. Cazarin, L. Costa, J. Pereira, M. Junior and A. Meirelles, *J. Food Res.*, 2020, **134**, 109125.

35 K. Zhao, K. Zhang, R. Li, P. Sang, H. Hu and M. He, *J. Mater. Chem. A*, 2021, **9**, 23714–23721.